Inorg. Chem. **2008**, *47*, 8444−8450

Inorganic Chemistry
Article

Forum

Isolation of Two-Dimensional 2:1 Cation-Ordered Perovskite Units by Anion Vacancy Ordering in $Ba_6Na_2Nb_2P_2O_{17}$

Xiaojun Kuang,[†] John B. Claridge,[†] Tim Price,[‡] David M. Iddles,[‡] and Matthew J. Rosseinsky*[,†]

Department of Chemistry, The University of Liverpool, Liverpool L69 7ZD, U.K., and Ceramic Division, Powerwave (U.K.) Ltd., Enterprise Drive, Station Road, Four Ashes, Wolverhampton WV10 7DF, U.K.

Received May 6, 2008

A new six-layer perovskite-related structure $Ba_6Na_2Nb_2M_2O_{17}$ (M = P, V), which consists of cubic (c) BaO_3 layers and oxygen-deficient pseudocubic (c′) BaO_2 layers stacked in the sequence c′ccccc, is presented. In $Ba_6Na_2Nb_2M_2O_{17}$, two-dimensional slabs of the well-known 2:1 octahedral cation-ordered perovskite motif are isolated between layers of tetrahedral units formed by anion vacancy ordering: two consecutive NbO_6 octahedral layers are sandwiched by two single NaO_6 octahedral layers, which, in turn, connect with two isolated MO_4 tetrahedral layers. Both oxides are derived from the 2:1 ordered perovskite structure (e.g., $Ba_3ZnTa_2O_9$) by ordered removal of O atoms in every sixth BaO_3 layer. Both materials exhibit a relative permittivity of ∼20−23, $Q \times f_0$ values of ∼7800−10600 GHz, and negative temperature coefficients of the resonant frequency of ∼−23 to −7 ppm/°C.

Introduction

Perovskite oxides are important in current solid-state chemistry and physics because of their diverse structural features and interesting physical and chemical properties, which result in a range of applications.[1] The cubic ABO_3 perovskite structure consists of a three-dimensional array of corner-sharing BO_6 octahedra, with the larger A cations in a 12-coordinate site, and arises from ordered B cation occupancy of 25% of the octahedral sites between close-packed AO_3 layers stacked along the ⟨111⟩ direction of the cubic unit cell. Cation site order[2] is important in perovskite-derived structures because it can control physical properties such as dielectric loss,[2] magnetoresistance,[3] magnetic order,[4,5] and ionic mobility.[6,7] Cation order on the octahedral B sites involves modulation of the occupancy of the sites between the AO_3 layers along the ⟨111⟩ stacking direction; with equal occupancy by two distinct cations, the 1:1 ordered $A_2B'B''O_6$ composition gives a six-layer cubic structure with alternating single octahedral B′ and B″ center layers (Figure 1a). A 2:1 ratio gives the $A_3B'B''_2O_9$ composition in a three-layer structure with alternation of single octahedral B′-centered layers and two consecutive octahedral B″-centered layers (Figure 1b). Control of the multiple cation order on the B-site sublattice of complex perovskites offers integration of distinct properties into oxide materials and is an important target.[8]

The occurrence of cation order is particularly significant in controlling microwave dielectric properties.[2,9] The key figures of merit for a microwave resonator are a high relative permittivity (ϵ_r) at microwave frequencies, a near-zero (±10 ppm/°C) value of the temperature coefficient of the resonant

---

* To whom correspondence should be addressed. E-mail: m.j.rosseinsky@liverpool.ac.uk.

† The University of Liverpool.

‡ Powerwave (U.K.) Ltd.

(1) Rao, C. N. R.; Raveau, B. *Transition Metal Oxides: Structure, Properties and Synthesis of Ceramic Oxides*, 2nd ed.; Wiley-VCH: New York, 1998.

(2) Davies, P. K. *Curr. Opin. Solid State Mater. Sci.* **1999**, *4*, 467–471.

(3) Huang, Y. H.; Karppinen, M.; Yamauchi, H.; Goodenough, J. B. *Phys. Rev. B* **2006**, *73*, 104408.

(4) Millange, F.; Caignaert, V.; Domenges, B.; Raveau, B.; Suard, E. *Chem. Mater.* **1998**, *10*, 1974–1983.

(5) Rodgers, J. A.; Battle, P. D.; Dupre, N.; Grey, C. P.; Sloan, J. *Chem. Mater.* **2004**, *16*, 4257–4266.

(6) Kim, G.; Wang, S.; Jacobson, A. J.; Yuan, Z.; Donner, W.; Chen, C. L.; Reimus, L.; Brodersen, P.; Mims, C. A. *Appl. Phys. Lett.* **2006**, 88.

(7) Harada, Y.; Hirakoso, Y.; Kawai, H.; Kuwano, J. *Solid State Ionics* **1999**, *121*, 245–251.

(8) Mallinson, P. M.; Allix, M. M. B.; Claridge, J. B.; Ibberson, R. M.; Iddles, D. M.; Price, T.; Rosseinsky, M. J. *Angew. Chem., Int. Ed.* **2005**, *44*, 7733–7736.

(9) Reaney, I. M.; Iddles, D. *J. Am. Ceram. Soc.* **2006**, *89*, 2063–2072.

10.1021/ic800788e CCC: $40.75

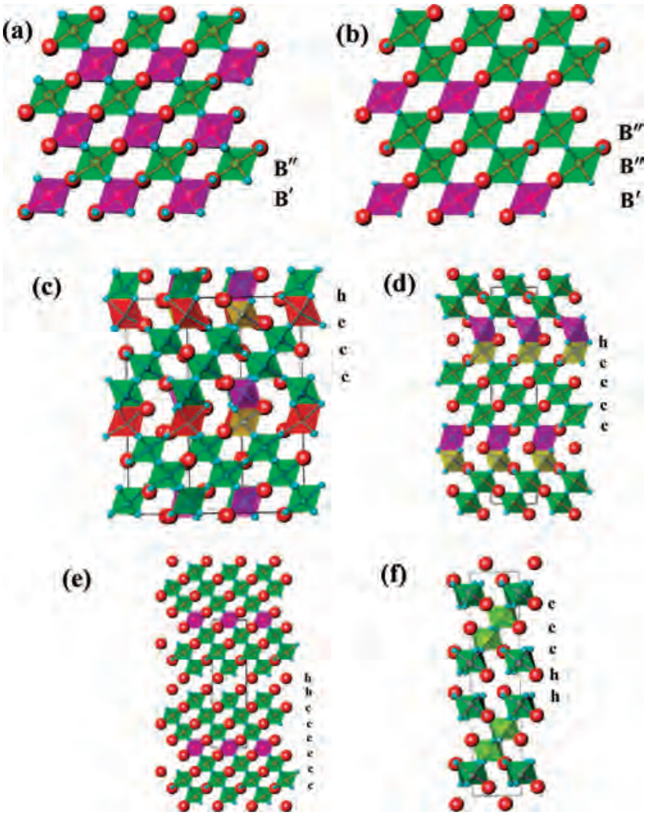

Figure 1. 1:1 $A_2B'B''O_6$ (a) and 2:1 $A_3B'B''_2O_9$ (b) octahedral B-site cation order patterns in the cubic perovskite structure: the ⟨111⟩ direction of the cubic cell is vertical. (c) Structure of the eight-layer $Ba_8ZnTa_6O_{24}$ hexagonal perovskites with partially ordered cation vacancies: the octahedral site in green is Ta (100%), red is an empty site, yellow is ~85% Ta plus vacancy, and purple is ~75% Zn and ~5% Ta plus vacancy. (d) Structure of the 10-layer $Ba_{10}Mg_{0.25}Ta_{7.9}O_{30}$ hexagonal perovskites, with a lower cation/vacancy order extent in the face-sharing octahedral site in purple compared with that for $Ba_8ZnTa_6O_{24}$: the octahedral site in green is Ta (100%), purple is ~35% Ta and ~6% Mg plus vacancy, and yellow is ~60% Ta and ~6% Mg plus vacancy. (e) Structure of $Ba_8CoNb_6O_{24}$ showing the isolation of Co^{2+} layers in pink by 18.8 Å from each other in a dielectric host of Nb^{5+} layers in green. (f) Structure model of the 10-layer titanate-based hexagonal perovskite, e.g., $BaLa_4Ti_4O_{15}$ and $La_5Zn_{0.5}Ti_{3.5}O_{15}$, where Zn prefers to occupy the central sites in yellow in a cubic block to the outer sites in green.

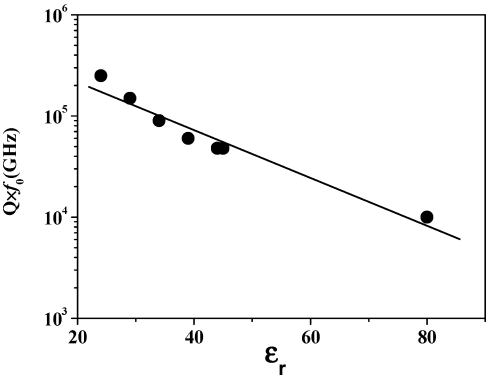

Figure 2. Correlation between $Q \times f_0$ and ϵ_r for zero τ_f commercial resonators. Reproduced with permission from ref 9. Copyright 2006 American Ceramic Society.

frequency (τ_f), and a low value of the dielectric loss (tan δ), often discussed in terms of $Q = (\tan\delta)^{-1} = f_0/\Delta f$ and $Q \times f_0$, where f_0 is the resonant frequency and Δf is the bandwidth of the resonant peak.[9] The high ϵ_r is important because it is inversely proportional to the resonator size. The temperature coefficient of the resonant frequency must be small to prevent network detuning with temperature fluctuations. The low loss corresponds to a small frequency width of the device resonance, which, in turn, allows efficient use of the available frequencies in cell-based telecommunication systems. Optimal materials for this application are d^0-based transition-metal oxides, many of which have the perovskite structure. Partially filled d shells can contribute loss mechanisms due to electronic conductivity: the multiple bonding characteristic of d^0 cations will enhance the electronic contribution to the polarizability and hence ϵ_r. The most significant materials with the highest value of Q are the 1:2 B-cation-ordered perovskites such as $Ba_3ZnTa_2O_9$ (BZT).[9,10] Here the values of $Q \times f_0$ for well-ordered BZT reach ~150 000 GHz with $\epsilon_r \sim 30$.[9−11] Niobates typically have higher ϵ_r[12] but lower Q (e.g., $\epsilon_r \sim 40$, $Q \times f_0 \sim 87\,000$ GHz for $Ba_3ZnNb_2O_9$[12,13]), attributed to the scaling of tan δ with $(\epsilon_r)^{-1}$, which is commonly observed (Figure 2). High permittivity is a particular characteristic of titanates, reflected by the site-disordered $0.7CaTiO_3{-}0.3NdAlO_3$ (CTNA) materials[14,15] ($\epsilon_r \sim 44$, $Q \times f_0 \sim 45\,000$ GHz[15]); $NdAlO_3$ doping lowers the permittivity but also τ_f of $CaTiO_3$; Q is low compared with BZT because of both the higher ϵ_r and the site disorder. The ceramic objects used as resonators need to be processed at high temperature for densification, and this processing considerably impacts the materials chemistry, which, in turn, controls the properties. In the case of BZT, it is the extent of cation order over the two distinct B sites in the structure that determines the properties. Materials with higher extents of order, and larger ordered domains, tend to have higher Q values.[10,11] This can be qualitatively associated with disorder, causing the loss associated with phonon resonances in the material to tail into the microwave region.[16,17] Davies and co-workers[18] have shown that dopants can produce high Q without large ordered domains, associating this with stabilization of the domain boundaries. The disordered cubic phase in BZT is reached above a $T_{o/d}$ (order−disorder transition temperature) of 1650 °C.[19] Because most commercial resonator processing operates completely below $T_{o/d}$, even materials that appear disordered to X-rays must have some extent of order over a short length scale, with the disorder corresponding to a high density of domain boundaries and domain walls. Order increases with the annealing temperature after calcination, so this is a kinetic

---

(10) Kawashima, S.; Nishida, M.; Ueda, I.; Ouchi, H. *J. Am. Ceram. Soc.* **1983**, *66*, 421–423.

(11) Desu, S. B.; O'Bryan, H. M. *J. Am. Ceram. Soc.* **1985**, *68*, 546–551.

(12) Lufaso, M. W. *Chem. Mater.* **2004**, *16*, 2148–2156.

(13) Nomular, S. *Ferroelectrics* **1983**, *49*, 61–70.

(14) Nenasheva, E. A.; Mudroliubova, L. P.; Kartenko, N. F. *J. Eur. Ceram. Soc.* **2003**, *23*, 2443–2448.

(15) Jancar, B.; Suvorov, D.; Valant, M.; Drazic, G. *J. Eur. Ceram. Soc.* **2003**, *23*, 1391–1400.

(16) Sagala, D. A.; Nambu, S. *J. Am. Ceram. Soc.* **1992**, *75*, 2573–2575.

(17) Wakino, K.; Murata, M.; Tamura, H. *J. Am. Ceram. Soc.* **1986**, *69*, 34–37.

(18) Davies, P. K.; Tong, J. Z.; Negas, T. *J. Am. Ceram. Soc.* **1997**, *80*, 1727–1740.

(19) Reaney, I. M.; Qazi, I.; Lee, W. E. *J. Appl. Phys.* **2000**, *88*, 6708–6714.

phenomenon; the detailed ordering kinetics can be followed in situ by synchrotron X-ray diffraction (XRD)[20] and reveal the extent of order present in the initial nuclei of the ordered state. The kinetic models followed for ordering are consistent with the presence of nuclei for the ordered state within the calcined precursor to the final cation-ordered product, in agreement with thermodynamic requirements given that all of the processing takes place below the order–disorder transition temperature. The activation energy of 311 kJ mol^{-1} for the ordering process agrees with the activation energies estimated for cation diffusion in oxides,[20] consistent with the need for cation site exchange to take place in the ordering process. Significantly, the ordered domain size varies in a nonmonotonic manner with the annealing temperature; 300 Å domains form at 1400 °C and 200 Å at 1500 °C. The change in the influence of the temperature on the domain size coincides with the observation of a different (exponential rather than a power law) kinetic expression for domain size dependence with time. This crossover is controlled by the extent of impurity contamination due to Zn loss, which becomes significant at higher temperature.[21,22]

The phases formed by this loss of Zn indicate how the cubic perovskite materials can be modified to afford further candidate microwave dielectrics, although at present none of these materials have the figures of merit found for the all-cubic perovskites. The Zn loss during the processing of BZT corresponds to the formation of B-cation-deficient $Ba_8ZnTa_6O_{24}$ (Figure 1c),[21,23,24] which has a mixed cubic–hexagonal stacking sequence where the B-site cation vacancies are accommodated in hexagonal perovskite layers introduced into the all-cubic stacking sequence to form an eight-layer repeat. By adjustment of the composition, other stacking sequences with longer repeat units, such as the 10-layer $Ba_{10}Mg_{0.25}Ta_{7.9}O_{30}$ (Figure 1d), are accessible.[25] These hexagonal vacancy-containing materials are attractive because they can attain high Q without requiring the high processing temperatures needed to order the cations in the cubic perovskite materials. In this case, the more extensively cation- and vacancy-ordered eight-layer material has considerably higher Q ($Q \times f_0 \sim 68\,224$ GHz for $Ba_8ZnTa_6O_{24}$[23]) than the 10-layer system ($Q \times f_0 \sim 33\,585$ GHz for $Ba_{10}Mg_{0.25}Ta_{7.9}O_{30}$).[25] Electron diffraction indicates that the ordering motifs established in three dimensions in the eight-layer systems are present only in two dimensions within the 10-layer materials; given the relationship between order and Q established in the all-cubic materials, it is possible that this is at the root of the poorer performance of the 10-layer materials. The 8- and 10-layer structures do not have the full site order of the two cations attainable in all-cubic BZT, which is associated with incomplete cation and vacancy ordering in the face-sharing octahedral layers. Mixed hexagonal–cubic stacking sequences can impose complete order when only corner-sharing octahedral sites are occupied; in $Ba_8CoNb_6O_{24}$, where two neighboring hexagonal layers produce a trimer of face-sharing octahedral sites with the central site vacant to avoid excessive repulsion, the resulting seven-layer unit of corner-sharing octahedra has Co^{2+} confined to the central layer, thus generating isolated layers of dielectric cations separated from each other by 18.8 Å within an ordered structure (Figure 1e).[8] There are titanate-based hexagonal perovskites, e.g., eight-layer $Ba_8Ti_3Nb_4O_{24}$ ($\epsilon_r \sim 48$, $Q \times f_0 \sim 21\,347$ GHz) (Figure 1c),[26] 10-layer $BaLa_4Ti_4O_{15}$ ($\epsilon_r \sim 46$, $Q \times f_0 \sim 46\,000$ GHz),[27] and $La_5Zn_{0.5}Ti_{3.5}O_{15}$ ($\epsilon_r \sim 37$, $Q \times f_0 \sim 23\,048$ GHz) (Figure 1f),[28] etc., which have higher ϵ_r than the cation- and vacancy-ordered hexagonal tantalates and niobates but also have lower Q, for reasons similar to those producing the contrasting properties of BZT and CTNA.

Given the importance of full cation site order within arrays of corner-sharing octahedra for high Q, the introduction of the cation-ordered motifs found in BZT as a subcomponent of a more complex structure is an interesting challenge. Here we report the isolation of a small subunit of the BZT high-Q structure as part of a more complex structure enforced by anion vacancy and cation site order in a six-layer perovskite-related structure $Ba_6Na_2Nb_2P_2O_{17}$.

Given the common occurrence of anion vacancy ordering in the perovskite structure, reduced cation coordination number to give tetrahedral or square-pyramidal B-site geometries is well-known in perovskite derivatives and can be coupled with multiple-B-site ordering patterns if vacancy containing BaO_{3-x} layers can be introduced into the stacking sequence.[29,30] Three-cation order in tetrahedral (T), pyramidal (P), and octahedral (O) sites according to the sequence $Na_{O/P}-V_T-V_T-Na_{O/P}-Mn_P$ (O/P denotes a mixed pyramidal and octahedral site) has been reported in the 15-layer structure $Ba_5Na_2MnV_2O_{13}$.[31] In this study, $Ba_6Na_2Nb_2P_2O_{17}$ exhibits B-site order of three distinct cations along the ⟨111⟩ pseudocubic direction to form octahedral and tetrahedral metal centers with the sequence $Na_O-P_T-P_T-Na_O-Nb_O-Nb_O$. Oxygen vacancy ordering within the cubic layer stacking sequence results in two isolated PO_4 tetrahedral layers, separating the 2:1 B-site ordered octahedral units from each other along the c axis. A polymorph of $Ba_6Na_2Nb_2V_2O_{17}$,[32] which can be made in the 12-layer hexagonal perovskite structure of $Ba_6Y_2Ti_4O_{17}$,[33] is isolated as an

---

(20) Mallinson, P. M.; Claridge, J. B.; Rosseinsky, M. J.; Ibberson, R. M.; Wright, J. P.; Fitch, A. N. *Chem. Mater.* **2007**, *19*, 4731–4740.

(21) Bieringer, M.; Moussa, S. M.; Noailles, L. D.; Burrows, A.; Kiely, C. J.; Rosseinsky, M. J.; Ibberson, R. M. *Chem. Mater.* **2003**, *15*, 586–597.

(22) Kawashima, S. *Am. Ceram. Soc. Bull.* **1993**, *72*, 120–126.

(23) Moussa, S. M.; Claridge, J. B.; Rosseinsky, M. J.; Clarke, S.; Ibberson, R. M.; Price, T.; Iddles, D. M.; Sinclair, D. C. *Appl. Phys. Lett.* **2003**, *82*, 4537–4539.

(24) Thirumal, M.; Davies, P. K. *J. Am. Ceram. Soc.* **2005**, *88*, 2126–2128.

(25) Mallinson, P.; Claridge, J. B.; Iddles, D.; Price, T.; Ibberson, R. M.; Allix, M.; Rosseinsky, M. J. *Chem. Mater.* **2006**, *18*, 6227–6238.

(26) Rawal, R.; Feteira, A.; Flores, A. A.; Hyatt, N. C.; West, A. R.; Sinclair, D. C.; Sarma, K.; Alford, N. M. *J. Am. Ceram. Soc.* **2006**, *89*, 336–339.

(27) Okawa, T.; Kiuchi, K.; Okabe, H.; Ohsato, H. *Jpn. J. Appl. Phys., Part 1* **2001**, *40*, 5779–5782.

(28) Kuang, X.; Allix, M. M. B.; Claridge, J. B.; Niu, H. J.; Rosseinsky, M. J.; Ibberson, R. M.; Iddles, D. M. *J. Mater. Chem.* **2006**, *16*, 1038–1045.

(29) Anderson, M. T.; Vaughey, J. T.; Poeppelmeier, K. R. *Chem. Mater.* **1993**, *5*, 151–165.

(30) Karen, P.; Woodward, P. M. *J. Mater. Chem.* **1999**, *9*, 789–797.

(31) Bendraoua, A.; Quarz, E.; Abraham, F.; Mentre, O. *J. Solid State Chem.* **2004**, *177*, 1416–1424.

(32) Quarez, E.; Abraham, F.; Mentre, O. *J. Solid State Chem.* **2003**, *176*, 137–150.

(33) Kuang, X.; Jing, X.; Loong, C. K.; Lachowski, E. E.; Skakle, J. M. S.; West, A. R. *Chem. Mater.* **2002**, *14*, 4359–4363.

isostructural phase with $Ba_6Na_2Nb_2P_2O_{17}$ in the present study. The electrical properties at alternating current (ac) and microwave frequencies of both materials are reported.

Experimental Section

Stoichiometric amounts of the starting materials $BaCO_3$ (Fisons, 99%+), $NaCO_3$ (Alfa Aesar, 99.997%), Nb_2O_5 (Sigma-Aldrich, 99.9%), $(NH_4)_2HPO_4$ (Alfa Aesar, 98%+), and V_2O_5 (Aldrich, 99.99%) were mixed with acetone in an agate mortar and pestle and calcined in an alumina crucible at 600 °C for 12 h. This calcined powder was pressed into pellets and fired at 800 °C for 12 h and at 1000 °C for 12 h with one intermediate grinding and pressing step to reach the final products of $Ba_6Na_2Nb_2M_2O_{17}$ (M = P, V). The phase purity of the final products was checked by XRD data with a Panalytical X'pert Pro Multi-Purpose X-ray diffractometer (Co Kα_1 radiation, λ= 1.789 01 Å), and data for Rietveld refinement were collected over a 2θ range of 10−120°. Time-of-flight neutron diffraction (ND) data were collected at room temperature on the POLARIS diffractometer at the ISIS facility, Rutherford Appleton Laboratories.

The pellets of $Ba_6Na_2Nb_2M_2O_{17}$ for electrical property measurement were made via the following processing. A ~20 g batch of the corresponding mixtures, where a higher purity raw $BaCO_3$ (99.997%, Alfa Aesar) material was used, was ball-milled overnight with magnesia-stablized zirconia beads in ethanol. After removal of ethanol, the dried powders were calcined at 600 °C for 12 h and at 700 °C for 6 h. The calcined powders were ball-milled overnight, dried again, and then pressed into pellets with a diameter of ~20 mm and a height of ~8 mm via use of a cold isostatic pressing facility. These pellets were sintered in 1000 °C for 12 h with a heating and cooling rate of 5 °C/min, which resulted in $Ba_6Na_2Nb_2P_2O_{17}$ pellets with ~92% of the X-ray theoretical density and $Ba_6Na_2Nb_2V_2O_{17}$ pellets with ~82% relative density. Both oxide pellets have a similar off-white color. Prolonged firing and higher temperatures up to 1200 °C did not improve the density. Regrinding the $Ba_6Na_2Nb_2V_2O_{17}$ pellet into fine powder and repressing and refiring also failed to improve the density.

Rietveld analysis was performed with both XRD and ND data using the *GSAS* software package[34] with the EXPGUI interface.[35] Bond valence sums (BVSs) were calculated by Brown and Altermatt's method.[36] Thermogravimetric analysis (TGA) was carried out from room temperature to 800 °C in air by using a EXSTAR6000 TGA-DTA instrument. Infrared absorption data were collected using a Perkin-Elmer RXI FTIR spectrometer in the 4000−400 cm^{-1} range on samples pressed with KBr.

Microwave dielectric properties were measured by a resonator reflection method.[37] Samples were placed in a 90 mm cubic cavity in the center of the volume. The cavity walls were silver-plated to minimize conductor losses at microwave frequency. Frequency and insertion loss were measured under calibration, allowing for an approximation of Q with minimal conductor and cable losses. ϵ_r was calculated from the measured frequency and sample volume. τ_f was measured from −40 to +100 °C. ϵ_r over the 10^3−10^6 Hz frequency range was measured by ac impedance spectroscopy (IS) measurement from room temperature to 120 °C with a Solartron 1255B frequency response analyzer and a Solartron 1296 dielectric interface, under a dry O_2 flow to exclude the influence of moisture on the permittivity (the pellet surface can absorb a small amount of water in air at low temperature, thus affecting the accuracy of the measurement). The temperature coefficient of dielectric permittivity was calculated as $\tau_\varepsilon = \Delta\varepsilon_r/(\Delta T\varepsilon_{r27\ °C})$, where $\varepsilon_{r27\ °C}$ is the permittivity at 27 °C. Pellets were coated with platinum paste and fired at 800 °C for 30 min prior to the IS measurement. From 350 to 700 °C, the ac conductivity was measured in air over 1−10^6 Hz.

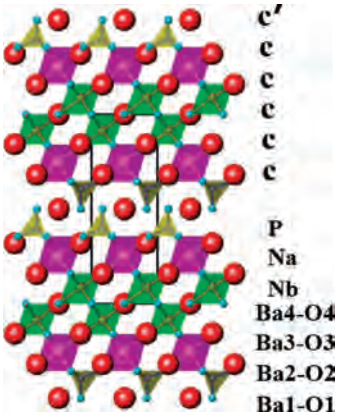

Figure 3. Projection along $[1\bar{2}0]$ of the structure of $Ba_6Na_2Nb_2P_2O_{17}$. Large red and small cyan spheres represent Ba and O, respectively. The consecutive Nb and Na octahedral block units are the same as those in the three-dimensional phase in Figure 1b. The layer marked c' corresponds to a layer with cubic stacking that contains oxygen vacancies (composition BaO_2 rather than BaO_3).

Results and Discussion

Crystal Structure of $Ba_6Na_2Nb_2P_2O_{17}$. Examination of the XRD data revealed that all of the reflections of $Ba_6Na_2Nb_2P_2O_{17}$ can be indexed with a six-layer hexagonal cell with a = 5.819 Å and c = 14.535 Å; the material is single phase. The absence of specific reflection conditions suggest a P lattice with trigonal $P3/P\bar{3}$-related and hexagonal $P6/P\bar{6}$-related space groups without glide planes. The six-layer structural model in Figure 3 with a sequence c'ccccc involving the introduction of ordered oxygen-deficient pseudocubic (c') BaO_2 layers can be constructed for $Ba_6Na_2Nb_2P_2O_{17}$ with the correct cell dimensions. This model corresponds to trigonal $P\bar{3}m1$, $P3m1$, $P321$, $P\bar{3}$, and $P3$ space groups. Therefore, the highest-symmetry $P\bar{3}m1$ space group was chosen for Rietveld refinement of both XRD and ND data; refinements in lower symmetry gave no improvement. These refinements confirmed the six-layer structure. The final structural parameters and selected bond lengths and angles for $Ba_6Na_2Nb_2P_2O_{17}$ from combined refinement against both XRD and ND data are listed in Tables 1 and 2, respectively, and Rietveld refinement of both XRD and ND data for $Ba_6Na_2Nb_2P_2O_{17}$ is shown in Figure 4.

$Ba_6Na_2Nb_2P_2O_{17}$ adopts a six-layer perovskite-related structure, which consists of cubic (c) BaO_3 and ordered oxygen-deficient pseudocubic (c') BaO_2 layers stacked according to the sequence c'ccccc (Figure 3). The structure of $Ba_6Na_2Nb_2P_2O_{17}$ is shown in Figure 5 with displacement ellipsoids. The refined site occupancies show complete ordering of Na^+, Nb^{5+}, and P^{5+} at the three crystallographically distinct B sites. The BVSs (in Table 1) agree well with

---

(34) Larson, A. C.; Von Dreele, R. B. *General Structure Analysis System (GSAS)*; Los Alamos National Laboratory Report LAUR 86-748; Los Alamos National Laboratory: Los Alamos, NM, 2004.

(35) Toby, B. H. *J. Appl. Crystallogr.* **2001**, *34*, 210–213.

(36) Brown, I. D.; Altermatt, D. *Acta Crystallogr., Sect. B* **1985**, *41*, 244.

(37) Kajfez, D.; Hwan, E. J. *IEEE Trans. Microwave Theory Tech.* **1984**, *32*, 666–670.

Table 1. Final Refined Structural Parameters for $Ba_6Na_2Nb_2P_2O_{17}$[a]

atom	site	x	y	z	U_{iso}(Å^2)	BVS[b]
Ba1	1a	0	0	0	0.0184(6)	1.75
Ba2	2d	2/3	1/3	0.17950(7)	0.0068(4)	2.11
Ba3	2d	1/3	2/3	0.34294(8)	0.0033(3)	2.01
Ba4	1b	0	0	0.5	0.0057(5)	2.13
Na	2c	0	0	0.2476(2)	0.0054(5)	1.48
Nb	2d	2/3	1/3	0.4125(1)	0.0021(2)	4.94
P	2d	1/3	2/3	0.1051(1)	0.0027(3)	4.76
O1	2d	1/3	2/3	−0.0002(1)	0.0168(4)	1.85
O2	6i	0.1886(1)	0.8114(1)	0.14322(6)	0.0123(2)	1.98
O3	6i	0.8220(1)	0.1780(1)	0.33963(6)	0.0079(2)	2.15
O4	3f	0.5	0.5	0.5	0.0076(3)	2.00

[a] $a = 5.81810(2)$ Å, $c = 14.53262(6)$ Å; space group, $P\bar{3}m1$; $Z = 1$; $R_{wp} = 3.50\%$, $R_p = 3.67\%$, $\chi^2 = 1.31$ (1.20 on XRD data and 1.66 on ND data) for 95 variables. [b] BVS denotes bond valence sum.

Table 2. Selected Bond Lengths (Å) and Angles (deg) for $Ba_6Na_2Nb_2P_2O_{17}$

bond	length	bond	length/angle
Ba1−O1 (×4)	3.35909(1)	Na−O2 (×3)	2.432(2)
Ba1−O1 (×2)	3.35908(1)	Na−O3 (×3)	2.237(2)
Ba1−O3 (×6)	2.819(1)	Nb−O3 (×3)	1.891(1)
Ba2−O1 (×1)	2.606(2)	Nb−O4 (×3)	2.106(9)
Ba2−O2 (×6)	2.9647(3)	P−O1 (×1)	1.530(3)
Ba2−O3 (×3)	2.805(1)	P−O2 (×3)	1.560(1)
Ba3−O2 (×3)	3.248(1)	O1−P−O2 (×3)	110.82(6)
Ba3−O3 (×6)	2.91167(6)	O2−P−O2 (×3)	108.09(6)
Ba3−O4 (×3)	2.8338(9)		
Ba4−O3 (×6)	2.941(1)		
Ba4−O4 (×6)	2.90905(1)		

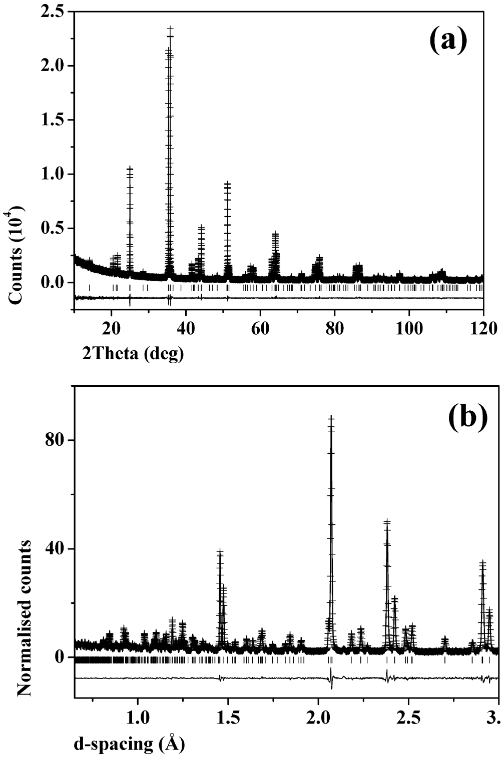

Figure 4. Rietveld refinement of ambient temperature XRD (a) and ND (b) data for $Ba_6Na_2Nb_2P_2O_{17}$. The Bragg reflection positions are shown by tick marks.

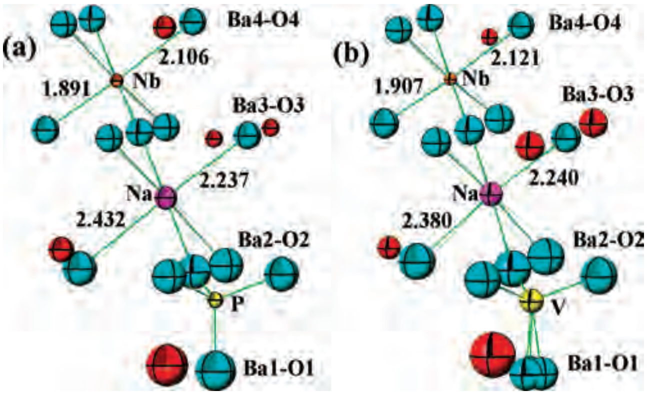

Figure 5. Displacement ellipsoid (99% probability) plots for the structures of $Ba_6Na_2Nb_2P_2O_{17}$ (a) and $Ba_6Na_2Nb_2V_2O_{17}$ (b) with Nb−O and Na−O bonds shown. Large red and small cyan spheres represent Ba and O, respectively. The c-axis direction is vertical. The O1 anion is positionally disordered in part b.

this assignment. Ordering of the anion vacancies into the c′ layers in the stacking sequence gives two neighboring layers of PO_4 tetrahedra. These tetrahedra are not connected to each other covalently because the O1 anions within the BaO_2 layers do not occupy the same positions as those in the BaO_3 layers; they are located directly above the P sites and constitute the terminal oxide anions of the phosphate groups. The c′ layers thus break the three-dimensional connectivity of the B sites within the perovskite structure, making the phosphate anions the boundary layers of the two-dimensional slabs from which the present structure is built. All of the polyhedral connectivity within these slabs is by corner-sharing because of the cubic-only AO_3 stacking sequence. The three basal O2 anions of the phosphate groups connect with a layer of NaO_6 octahedra, which are followed by two consecutive corner-shared NbO_6 octahedral layers. The oxygen vacancy ordering and size matching of Na^+, Nb^{5+}, and P^{5+} at the different sites are responsible for this three-cation B-site order within the two-dimensional structural units. The structure produces proximity of the tetrahedral PO_4 units with their short P−O bonds to the large NaO_6 octahedra with their weaker metal−oxygen interactions. The pair of corner-sharing layers of NbO_6 units feature displacement of the Nb cations away from the triangle of oxide anions shared with the neighboring Nb layer toward the oxide anions coordinated to the Na layer (Figure 5). The competition between the strength of the P−O and Nb−O interactions gives the Na^+ cation a distorted environment (Figure 5), which is consistent with those found in $Ba_5Na_2MnV_2O_{13}$[31] and $Ba_6Na_2Ru_2V_2O_{17}$.[32]

TGA on the phase-pure $Ba_6Na_2Nb_2P_2O_{17}$ sample did not reveal any apparent mass loss during heating from ambient temperature to 800 °C, which indicates that there is no water absorbed by the phosphate units. This result is consistent with infrared data, which did not show typical hydroxyl vibration absorption bands. The bands in the 1200−900 cm^{-1} range (in Figure S1 in the Supporting Information) can be ascribed to the vibration of tetrahedral PO_4 units.

Crystal Structure of $Ba_6Na_2Nb_2V_2O_{17}$. Combined Rietveld refinement of both XRD and ND data from $Ba_6Na_2Nb_2V_2O_{17}$ was performed based on the structure model of $Ba_6Na_2Nb_2P_2O_{17}$. $Ba_3V_2O_8$ (∼2.5 wt %) was observed as a minor second phase and was added into the refinement. The oxygen O1 in the c′ layers was initially placed at the ideal site, 2d on the 3-fold axis, which resulted in a relatively high atomic displacement factor (Å^2) U_{iso} ∼

Table 3. Final Refined Structural Parameters for $Ba_6Na_2Nb_2V_2O_{17}$[a]

atom	site	*x*	*y*	*z*	U_{iso} (Å^2)	occupancy	BVS[b]
Ba1	1a	0	0	0	0.0252(7)	1	1.80
Ba2	2d	2/3	1/3	0.18574(9)	0.0065(3)	1	1.98
Ba3	2d	1/3	2/3	0.3479(1)	0.0102(4)	1	1.89
Ba4	1b	0	0	0.5	0.0035(4)	1	2.07
Na	2c	0	0	0.2526(2)	0.0065(4)	1	1.55
Nb	2d	2/3	1/3	0.41385(9)	0.0021(2)	1	4.73
V	2d	1/3	2/3	0.1051(3)	0.007(1)	1	5.11
O1	6i	0.3123(4)	0.6246(9)	−0.0091(2)	0.0131(7)	1/3	1.88
O2	6i	0.1755(2)	0.8245(2)	0.14615 (6)	0.0164(2)	1	2.06
O3	6i	0.8235(1)	0.1765(1)	0.34314(7)	0.0107(2)	1	2.07
O4	3f	0.5	0.5	0.5	0.0089(3)	1	1.95

[a] $a = 5.87077(2)$ Å, $c = 14.79803(6)$ Å; space group, $P\bar{3}m1$; $Z = 1$; $R_{wp} = 4.42\%$, $R_p = 4.86\%$, $\chi^2 = 2.36$ (2.30 on XRD data and 2.57on ND data) on 24 variables. [b] BVS denotes bond valence sum.

Table 4. Selected Bond Lengths (Å) and Angles (deg) for $Ba_6Na_2Nb_2V_2O_{17}$

bond	length	bond	length/angle
Ba1−O1 (×4)	3.504(2)	Na−O2 (×3)	2.380(3)
Ba1−O1 (×2)	3.178(4)	Na−O3 (×3)	2.240(2)
Ba1−O3 (×6)	2.804(1)	Nb−O3 (×3)	1.907(1)
Ba2−O1 (×1)	2.624(3)	Nb−O4 (×3)	2.1207(8)
Ba2−O2 (×6)	2.9946(3)	V−O1 (×1)	1.702(4)
Ba2−O3 (×3)	2.823(2)	V−O2 (×3)	1.716(2)
Ba3−O2 (×3)	3.389(2)	O1−V−O2 (×2)	114.2(2)
Ba3−O3 (×6)	2.93793(7)	O1−V−O2 (×1)	103.5(2)
Ba3−O4 (×3)	2.818(1)	O2−V−O2 (×3)	108.2(1)
Ba4−O3 (×6)	2.934(1)		
Ba4−O4 (×6)	2.93538(1)		

0.031. This was not altered by refinement in lower-symmetry space groups. A difference Fourier map calculated with all of the atoms excluding O1 confirmed the scattering density around the ideal 2d site without indicating any additional positions. The refined anisotropic displacement factors for O1, $U_{11} = U_{22} \sim 0.043$, $U_{33} \sim 0.0074$, $U_{12} \sim 0.022$, and $U_{13} = U_{23} = 0$, suggest significant displacement in the *ab* plane compared with the *c* direction. This anisotropic displacement agrees well with the environment (Ba1−O1 ~ 3.390 Å) in the c′-BaO_2 layers, which are not close-packed, permitting large displacements in the *ab* plane. Therefore, the O1 site was displaced from the 3-fold axis to the general 6i position with an occupancy of 1/3, which led to a reasonable $U_{iso} \sim 0.013$ Å.^{2} The distance between the 6i and 2d sites is ~0.21 Å. Such oxide ion disorder in the c′-BaO_2 layer has been observed in hexagonal $Ba_7Y_2Mn_3Ti_2O_{20}$,[38] which is a mixed conductor. In $Ba_6Na_2Nb_2P_2O_{17}$, the refinement also revealed similar anisotropic displacement ($U_{11} = U_{22} \sim 0.024$, $U_{33} \sim 0.0054$, $U_{12} \sim 0.012$, and $U_{13} = U_{23} = 0$) for O1 because of the absence of close packing in the c′ layer (Ba1−O1 ~ 3.360 Å), although the refined isotropic displacement factor for O1 is reasonable, ~0.014, suggesting that the site splitting model for O1 is not necessary here. The shorter P−O bond suppresses the more extensive in-plane displacements found in the vanadate case. The refined structural parameters, and selected bond lengths and angles for $Ba_6Na_2Nb_2V_2O_{17}$ are listed in Tables 3 and 4, respectively. The Rietveld refinement plot of the ND data for $Ba_6Na_2Nb_2V_2O_{17}$ is shown in Figure 6.

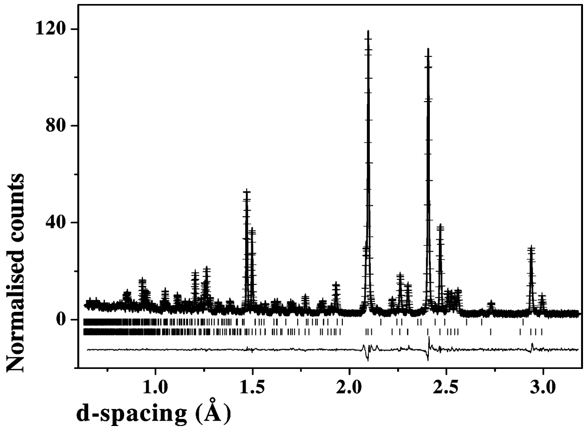

Figure 6. Rietveld refinement of ND data (POLARIS, backscattering detectors) for $Ba_6Na_2Nb_2V_2O_{17}$. Bragg reflection positions of the main phase $Ba_6Na_2Nb_2V_2O_{17}$ (lower) and the minor impurity $Ba_3V_2O_8$ (upper) are shown as tick marks.

The same B-site and anion vacancy ordering occurs in $Ba_6Na_2Nb_2V_2O_{17}$ with the sequence $Na_O{-}V_T{-}V_T{-}Na_O{-}Nb_O{-}Nb_O$ along the ⟨111⟩ pseudocubic direction, as observed in the phosphate case. The Rietveld refinement using the mixed hexagonal−cubic structure model of $Ba_6Y_2Ti_4O_{17}$[33] with hexagonal ABA stacking (denoted as h) of BaO_3 layers introduced to give the sequence $(c'cchcc)_2$, was not successful on the $Ba_6Na_2Nb_2V_2O_{17}$ sample studied here, suggesting that the present material is a second polymorph with all cubic-stacked BaO_3 and BaO_2 layers.

This cation order observed in $Ba_6Na_2Nb_2M_2O_{17}$ (M = P, V) results in the separation of the octahedral Nb^{5+} bilayer blocks by ~1.5 nm along the *c* axis. The strong charge difference between Nb^{5+} and Na^+ imposes the 2:1 ordering within the octahedral subunits of the structure, separated from each other by the anion-deficient BaO_2 layers, which generate the tetrahedral sites bounding the six-B-site repeat. The cation octahedral site order in $Ba_6Na_2Nb_2M_2O_{17}$ (M = V, P) makes this structure a derivative of the 2:1 B-site ordered cubic perovskite. The 2:1 units are not continuous, as in the microwave dielectric $Ba_3ZnTa_2O_9$, but extend only in two dimensions, with the bounding MO_4 units separating neighboring modules of the same vertical size as the unit cell along the stacking direction. This structure can also be viewed as consisting of alternative 2:1 ordered perovskite blocks $(Ba_3NaNb_2O_9)^-$ and 2:1 ordered perovskite-related blocks $(Ba_3NaM_2O_8)^+$ with oxygen vacancies ordered along the *c* direction.

Electrical Properties of $Ba_6Na_2Nb_2M_2O_{17}$. The XRD data of the $Ba_6Na_2Nb_2M_2O_{17}$ ceramics for electrical property measurement suggested that the $Ba_6Na_2Nb_2P_2O_{17}$ pellets contained minor second-phase $Ba_5P_3O_{12}OH$ (~5 wt %) and the Ba6-

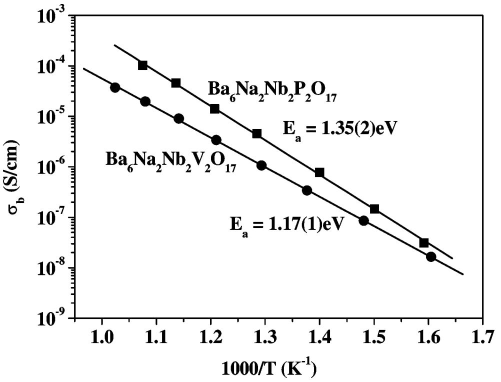

Figure 7. Arrhenius plots of bulk conductivity for $Ba_6Na_2Nb_2M_2O_{17}$.

$Na_2Nb_2V_2O_{17}$ pellets have phase formation similar to that in the powder sample for structural characterization. The room temperature relative permittivity values over the 10^3-10^6 Hz range are 20(1) for the $Ba_6Na_2Nb_2P_2O_{17}$ ceramics and 23(1) for the $Ba_6Na_2Nb_2V_2O_{17}$ ceramics, consistent with those, 20(2), found at microwave frequencies for both materials within experimental error. These agree well with those (20.11 and 20.37 for $Ba_6Na_2Nb_2P_2O_{17}$ and $Ba_6Na_2Nb_2V_2O_{17}$, respectively) estimated by using the Clausius−Mossotti relationship[39] with Shannon ionic polarizabilities[39] for all of the ions except $\alpha(Nb^{5+})$, for which the updated value of 4.65 Å^3 proposed by Lufaso[12] from the 2:1 ordered perovskite materials was used. The temperature coefficients of dielectric permittivity, τ_ε (ppm/°C), are ~-343 for $Ba_6Na_2Nb_2P_2O_{17}$ and ~-522 for $Ba_6Na_2Nb_2V_2O_{17}$. The temperature coefficients of the resonant frequency, τ_f (ppm/°C), are −23 for $Ba_6Na_2Nb_2P_2O_{17}$ and −7 for $Ba_6Na_2Nb_2V_2O_{17}$. Both materials exhibit insulating behavior, and their bulk conductivities from the ac impedance spectra (see Figure S2 in the Supporting Information) vary from 10^{-8} to 10^{-5} S/cm in the high-temperature region 350−700 °C with activation energies (eV) of 1.35(2) for $Ba_6Na_2Nb_2P_2O_{17}$ and 1.17(1) for $Ba_6Na_2Nb_2V_2O_{17}$ (in Figure 7). The $Q \times f_0$ values (GHz) measured at ~4 GHz for the as-sintered ceramics are 7800 for $Ba_6Na_2Nb_2P_2O_{17}$ and 8000 for $Ba_6Na_2Nb_2V_2O_{17}$, which were slightly improved via further annealing at 600 °C for 30 h to 8200 and 10 600, respectively. The $Q \times f_0$ values of both materials are comparable to 1:2 ordered Sr-based perovskite dielectrics, e.g., $Sr_3ZnNb_2O_9$,[40] but apparently inferior to those for the 1:2 ordered Ba-based perovskite dielectrics, e.g., $Ba_3B'B''_2O_9$ ($B' = Zn^{2+}, Mg^{2+}, Co^{2+}$, $B'' = Nb^{2+}, Ta^{5+}$).[9,41] Such low quality factors for these two materials may reflect the need to optimize extrinsic factors associated with the resonator processing, e.g., the likely Na loss due to volatilization of Na during the synthesis, the existence of minor second phases ($Ba_5P_3O_{12}OH$ in the $Ba_6Na_2Nb_2P_2O_{17}$ pellets and $Ba_3V_2O_8$ in the $Ba_6Na_2Nb_2V_2O_{17}$ pellets), and the porosity in the $Ba_6Na_2Nb_2V_2O_{17}$ pellets, which have ~82% relative density.

Conclusion

A six-layer perovskite-related structure $Ba_6Na_2Nb_2M_2O_{17}$ (M = P, V), featuring the isolation of two-dimensional 2:1 ordered perovskite units by oxygen vacancy ordering, is identified in two isostructural materials. The $Ba_6Na_2Nb_2M_2O_{17}$ materials show modest permittivity of ~20−23, low $Q \times f_0$ values of ~7800−10600 GHz, and negative temperature coefficients of the resonant frequency of −23 to −7 ppm/°C. Such isolation of the 2:1 ordered perovskite units in $Ba_6Na_2Nb_2M_2O_{17}$ imposed by oxygen vacancy ordering implies that oxygen vacancy defects could be significant in controlling the kinetics of site order of complex perovskite microwave dielectrics, playing a role similar to that demonstrated for Zn loss in BZT[21,22] and the nonstoichiometry in $Ba_3MgTa_2O_9$,[42] affecting the extent of order via control of the kinetic processes. The isolation of the multiple-B cation-ordered perovskite-related structure $Ba_6Na_2Nb_2M_2O_{17}$ suggest that a family of such six-layer structures with enhanced diversity of B cations can be accessed for new microwave dielectric oxides. The structures of the two $Ba_6Na_2Nb_2M_2O_{17}$ phases reported here and the $Ba_5Na_2MnV_2O_{13}$ materials from ref 31 form a new family of perovskite-related structures $A_nB_nO_{3n-\delta}$ with the sequence $(c'c_{n-1})_m$ (n = 5, 6; m = 1, 3). The introduction of vacancy ordering driven by species that strongly favor tetrahedral coordination allows the spatial isolation of fragments of extended cation-ordered motifs that are important in extended three-dimensional functional perovskite oxides. The versatility of complex anion species such as carbonate and sulfate for incorporation in low-coordination environments in perovskite-related structures[43,44] suggests that a broad family of compounds based on the isolation of cation-ordered fragments of three-dimensional perovskites may be accessible, extending to larger slabs of common cation-ordered motifs isolated by vacancy-ordered layers.

Acknowledgment. The authors thank EPSRC (EP/C511794) for support and Dr. R. I. Smith for his help with the ND data collection.

Supporting Information Available: Infrared absorption data of $Ba_6Na_2Nb_2P_2O_{17}$, ac impedance data of $Ba_6Na_2Nb_2M_2O_{17}$, and a crystallographic information file in CIF format. This material is available free of charge via the Internet at http://pubs.acs.org.

IC800788E

---

(38) Kuang, X.; Allix, M.; Ibberson, R. M.; Claridge, J. B.; Niu, H. J.; Rosseinsky, M. J. *Chem. Mater.* **2007**, *19*, 2884–2893.

(39) Shannon, R. D. *J. Appl. Phys.* **1993**, *73*, 348–366.

(40) Thirumal, M.; Jawahar, I. N.; Surendiran, K. P.; Mohanan, P.; Ganguli, A. K. *Mater. Res. Bull.* **2002**, *37*, 185–191.

(41) Hughes, H.; Iddles, D. M.; Reaney, I. M. *Appl. Phys. Lett.* **2001**, *79*, 2952–2954.

(42) Surendran, K. P.; Sebastian, M. T.; Mohanan, P.; Moreira, R. L.; Dias, A. *Chem. Mater.* **2005**, *17*, 142–151.

(43) Francesconi, M. G.; Greaves, C. *Supercond. Sci. Technol.* **1997**, *10*−A37.

(44) Greaves, C.; Kissick, J. L.; Francesconi, M. G.; Aikens, L. D.; Gillie, L. J. *J. Mater. Chem.* **1999**, *9*, 111–116.